

An external-shock model for GRB afterglow 130427A

A. Panaitescu, W.T. Vestrand, P. Woźniak

Space & Remote Sensing, MS B244, Los Alamos National Laboratory, Los Alamos, NM 87545, USA

ABSTRACT

The complex multiwavelength emission of GRB afterglow 130427A (monitored in the radio up to 10 days, in the optical and X-ray until 50 days, and at GeV energies until 1 day) can be accounted for by a hybrid reverse-forward shock synchrotron model, with inverse-Compton emerging only above a few GeV. The high ratio of the early optical to late radio flux requires that the ambient medium is a wind and that the forward-shock synchrotron spectrum peaks in the optical at about 10 ks. The latter has two consequences: the wind must be very tenuous and the optical emission before 10 ks must arise from the reverse-shock, as suggested also by the bright optical flash that Raptor has monitored during the prompt emission phase (< 100 s). The VLA radio emission is from the reverse-shock, the Swift X-ray emission is mostly from the forward-shock, but the both shocks give comparable contributions to the Fermi GeV emission. The weak wind implies a large blast-wave radius ($8t_{\text{day}}^{1/2}$ pc), which requires a very tenuous circumstellar medium, suggesting that the massive stellar progenitor of GRB 130427A resided in a super-bubble.

Key words: radiation mechanisms: non-thermal – relativistic processes – shock waves

1 INTRODUCTION

Gamma-Ray Burst (GRB) 130427A may well be the burst with the most comprehensive afterglow follow-up, its multiwavelength monitoring covering radio, optical, X-ray, and γ -ray frequencies, and extending from seconds to tens of days after trigger. The X-ray *prompt* emission (up to 100 s) was accompanied by the second brightest optical flash, monitored by Raptor (Vestrand et al 2013), with the optical afterglow light-curve displaying a steepening at 300 s and a flattening at 10 ks. The Swift X-ray light-curve (X-ray light-curve repository – Evans et al 2009) is consistent with a single power-law from 500 s to 5 Ms. The Fermi-LAT γ -ray light-curve (Tam et al 2013) displays a peak at 10–20 s, simultaneous with the optical flash peak, and a steepening at 550–800 s (Zhu et al 2013). The VLA radio light-curves (Laskar et al 2013) display a slow decay at 1–10 day.

With such a rich dataset, GRB afterglow 130427A demands a theoretical interpretation, done here in the framework of the external-shock model (Mészáros & Rees 1997) where some relativistic ejecta, produced by the black-hole resulting from the core-collapse of a massive star, drive a *forward-shock* into the ambient medium while the ejecta are energized by the *reverse-shock*. The synchrotron and inverse-Compton emissions from both shocks are calculated assuming that electrons and magnetic field acquire a certain fraction of the post-shock energy. The shock-accelerated electrons are assumed to have a power-law distribution with

energy (hence the synchrotron and inverse-Compton spectra are also power-laws), with a break at the cooling energy (where the radiative-loss timescale equals the shock age).

Analytical treatments for the forward-shock emission have been provided by Mészáros & Rees (1997), Sari, Piran & Narayan (1998), Waxman, Kulkarni & Frail (1998), Granot, Piran & Sari (1999), Wijers & Galama (1999), Chevalier & Li (2000), Panaitescu & Kumar (2000), and for the reverse-shock by Kobayashi (2000). Both shocks have been studied with 1-dimensional hydrodynamical codes by Panaitescu & Mészáros (1998) and Kobayashi & Sari (2000), the former focusing on the two-shock synchrotron and inverse-Compton emission, the latter on the dynamics of the shocks.

To model the multiwavelength emission of GRB afterglow 130427A, we employ a 1-dimensional code that follows the ejecta-medium interaction, with the dynamics of each shock calculated from conservation of energy and using the shock jump-conditions (Blandford & McKee 1976). After the onset of deceleration, the dynamics of the forward-shock is determined by the ejecta initial energy, injected energy (Rees & Mészáros 1998), and ambient medium density. The dynamics of the reverse-shock is determined by that of the shocked fluid and two properties of the incoming ejecta: their energy and Lorentz factor. Here, we consider that the ejecta add energy to the blast-wave as a power-law in observer time and that they have a single Lorentz factor. The

self-absorption and cooling frequencies of the synchrotron spectrum and the inverse-Compton parameter are calculated self-consistently from the electron distribution and the magnetic field strength (Panaiteescu & Mészáros 2000). Radiative losses are also calculated from the electron distribution, but they are negligible for the following best-fit models. The emissions from both shocks are integrated over their motion and over the angle at which the fluid moves relative to the direction toward the observer. More details about this numerical model and its application to the multiwavelength emission of ten GRB afterglows are given in Panaiteescu (2005).

2 REVERSE-FORWARD (EXTERNAL) SHOCK MODEL

2.1 Closure relations for forward-shock light-curves suggest a homogeneous medium

The choice of the model features that may accommodate the temporal decay of the broadband emission of GRB afterglow 130427A starts with the X-ray light-curve because its temporal decay index ($F \propto t^{-\alpha}$) and spectral slope ($F_\nu \propto t^{-\beta}$) are the best determined: $\alpha_x = 1.36 \pm 0.01$ at 20 ks – 5 Ms (Fig 1) and $\beta_x = 0.79 \pm 0.16$ at mean time 24 ks (Kennea et al 2013). These lead to $\alpha_x - 1.5\beta_x = 0.18 \pm 0.24$, which is compatible with the value expected (zero) for the synchrotron emission from the forward-shock interacting with a homogeneous medium and for the X-ray being below the cooling frequency ν_c of the synchrotron spectrum.

As the optical flux also decays at that time, the optical must be above the peak energy ν_p of the synchrotron spectrum, hence optical and X-ray are in the same spectral regime: $\nu_p < \nu_o(2\text{ eV}) < \nu_x(10\text{ keV}) < \nu_c$. Consequently, the intrinsic afterglow optical flux can be calculated from the X-ray flux: $F_o = F_x(\nu_o/\nu_x)^{\beta_x}$. For instance, the observed $F_{10\text{ keV}}(54\text{ ks}) = 1.4\text{ }\mu\text{Jy}$ implies that $F_{2\text{ eV}}(54\text{ ks}) = 1.2\text{ mJy}$, which is a factor 2.5 larger than the measured $F_{2\text{ eV}}(53\text{ ks}) = 0.47\text{ mJy}$, requiring $A_R = 1\text{ mag}$ of dust extinction in the host galaxy.

The 10 keV – 100 MeV spectral slope $\beta_{xg}(43\text{ ks}) \simeq 0.89 \pm 0.09 \gtrsim \beta_x$ indicates that ν_c is well above 10 keV. That the LAT flux decays slower than in the X-ray ($\alpha_g = 1.22 \pm 0.09$ at 500 s – 50 ks) indicates that ν_c is below the LAT range (otherwise, for $\nu_c > 100\text{ MeV}$, the model expectation is $\alpha_x = \alpha_g$) and that the electron radiative cooling is dominated by inverse-Compton scatterings (otherwise, for synchrotron-dominated electron cooling, $\nu_c \propto t^{-1/2}$ and $\alpha_g - \alpha_x = -0.5(d \log \nu_c / d \log t) = 1/4$, incompatible with the observed $\alpha_g \lesssim \alpha_x$). More exactly, for a Compton-dominated electron cooling, the decay index of the synchrotron flux above ν_c is $\alpha = 3p/4 - 1/(4-p) = 1.27$, which matches well the observed α_g , with $p = (4\alpha_x + 3)/3 = 2.8$ being the exponent of the power-law distribution of electrons with energy ($dN/d\epsilon \propto \epsilon^{-p}$) that is required by the forward-shock model, given the measured flux decay index α_x below the cooling frequency.

In summary, the optical, X-ray, and γ -ray fluxes of GRB afterglow 130427A, their decay indices, and the X-ray spectral slope, require that $\nu_p < \nu_o < \nu_x < \nu_c < \nu_g$, if the afterglow emission is synchrotron from the forward-shock.

2.2 External medium is not homogeneous

Under the assumption that the two microphysical parameters of the forward-shock (ϵ_B and ϵ_i) that quantify the post-shock fractional energy in the magnetic field and in electrons are constant, the forward-shock synchrotron light-curve at any frequency below the optical can be easily calculated from the optical light-curve, using the expected evolution of the synchrotron peak flux ($F_p = \text{const}$) and peak energy ($\nu_p \propto t^{-3/2}$) for a homogeneous medium. If ν_p crosses the optical at some time t_o , yielding an optical flux F_o , then the radio flux at frequency $\nu_r < \nu_p$ is

$$F_r(t) = F_p(\nu_r/\nu_p)^{1/3} = F_o(t_o)(t/t_o)^{1/2}(\nu_r/\nu_o)^{1/3} \propto t^{1/2} \quad (1)$$

Here, $F_o(t_o) \simeq 5(t_o/10\text{ ks})^{-\alpha_o}\text{ mJy}$ is the intrinsic optical light-curve after 10 ks (corrected for the above-inferred host extinction of $A_R = 1\text{ mag}$) and $\alpha_o = 1.36$ (the forward-shock model requires that $\alpha_o = \alpha_x$). The largest t_o required by equation (1) arises from the radio measurement with the highest $\nu_r^{1/3}t^{1/2}/F_r$; taking the $F_{36\text{ GHz}}(9.7\text{ d}) = 0.43\text{ mJy}$ measurement as an upper limit for the forward-shock radio flux, implies $t_o \gtrsim 23\text{ ks}$.

This means that, for the forward-shock emission (that accommodates the observed optical flux) not to exceed the measured radio fluxes, the synchrotron peak should cross the optical at 23 ks. Conversely, if the synchrotron peak crossed the optical before 23 ks, then the synchrotron flux from the forward-shock would violate VLA measurements. That may be avoided if the magnetic field parameter ϵ_B decreases (roughly as t^{-1}), and if energy injection in the forward-shock is allowed (to match the optical and X-ray flux decays at 1–10 day, which are faster when ϵ_B decreases), but this scenario requires fine-tuning and we do not pursue it.

Fig 1 illustrates the failure of the forward-shock synchrotron model with a homogeneous medium to accommodate simultaneously the radio, optical, X-ray, and γ -ray fluxes of GRB afterglow 130427A: while it can explain the optical afterglow emission after 10 ks and the X-ray flux at 50 s – 5 Ms (excluding the second GRB pulse, which is a feature that cannot be accounted for by any type of external shock), this model over-predicts either the lowest or the highest frequency data.

2.3 Wind-like medium and forward-shock emission for the late optical afterglow

The closure relation $\alpha_x - 1.5\beta_x = 0.18 \pm 0.24$ is also compatible with the forward-shock model expectation for a wind-like medium (with an $n \propto r^{-2}$ particle density distribution with radius) and for X-ray below the cooling frequency, provided that there is an energy injection in the forward-shock that slows its deceleration and the decay of the afterglow X-ray flux. If that energy injection is parametrized as $E \propto t^e$ in observer time (a power-law flux decay requires that the dynamics of the forward-shock is a power-law in observer time), then $\alpha_x - 1.5\beta_x = [1 + (\beta_x + 1)e]/2$, from where $e = 3 - 2(\alpha_x + 1)/(\beta_x + 1) = 0.36 \pm 0.23$.

Numerically, we find that the best-fit to the X-ray emission after 500 s (including all the GeV data and the optical

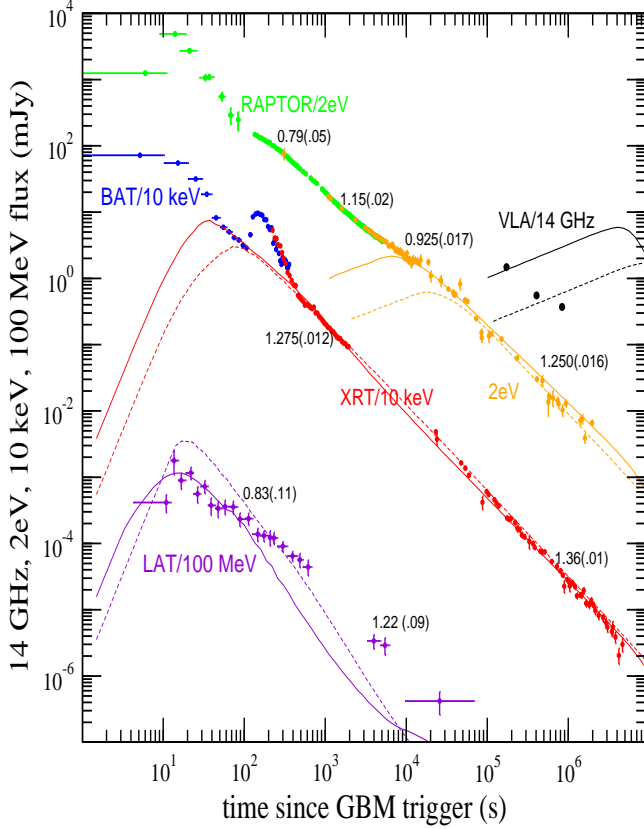


Figure 1. Multiwavelength light-curves for GRB 130427A and the synchrotron forward-shock/homogeneous-medium model best-fit to the radio, optical after 10 ks, X-ray after 50 s, and γ -ray measurements (the second X-ray pulse at 100–400 s is not included in the fit). Numbers adjacent to light-curves give the local power-law flux decay index (and its 1σ uncertainty).

Solid lines are for a model excluding radio measurements; the peak of the synchrotron spectrum crosses the R-band (2 eV) at 10 ks and the model over-predicts some of the VLA radio measurements at 1–10 day and 1–90 GHz (as expected from eq 1). The parameters of this model are: ejecta initial kinetic energy $E_0 = 3.10^{53}$ erg/sr, ejecta initial Lorentz factor $\Gamma_0 = 850$ (to yield a 20 s peak for the 100 MeV flux, when the ejecta deceleration begins), ambient medium density $n = 2.10^{-3}\text{cm}^{-3}$, magnetic-field parameter $\epsilon_B = 10^{-4}$, electron minimum-energy parameter $\epsilon_i = 0.11$, index of electron power-law distribution with energy $p = 2.5$, host dust-extinction $A_V = 1.3$.

Dashed lines are for a model including the radio measurements, which forces the peak of the synchrotron spectrum to be higher (crossing the optical at 20 ks). This model still over-predicts some radio measurements as well as the γ -ray flux measured by LAT during the prompt phase. Its parameters are similar to the solid lines model, the most notable difference being $\epsilon_i = 0.23$.

after 10 ks) has $e = 0.30$ and that forward-shock energy should increase by a factor $E_i/E_0 = 3$ until $t_e \simeq 1$ Ms, to account for the observed X-ray flux decay. That means that the energy added to the forward-shock mitigates its deceleration after $t_i = t_e(E_0/E_i)^{1/e} = 20$ ks.

It is important to note that the forward-shock interacting with a wind-like medium does not produce more radio emission than measured because the synchrotron peak flux decreases as $F_p \propto t^{-1/2}$ (instead of being constant, as for a

homogeneous medium). The evolution of the synchrotron peak energy is the same as for a homogeneous medium ($\nu_p \propto t^{-3/2}$), hence the radio flux expected from the optical emission is

$$F_r(t) = F_p(\nu_r/\nu_p)^{1/3} = F_o(t_o)(\nu_r/\nu_o)^{1/3} \propto t^0 \quad (2)$$

Then, $F_o(t_o) \simeq 2(t_o/10 \text{ ks})^{-1.36}$ mJy and $F_{36 \text{ GHz}}(9.7 \text{ d}) = 0.43$ mJy require that the time when the synchrotron peak crosses the optical is $t_o \gtrsim 3$ ks. That brief flattening seen in the optical light-curve at 10 ks could be due to ν_p crossing the optical and is compatible with $t_o \gtrsim 3$ ks.

The best-fit to the optical data after 10 ks, the X-ray after 500 s, and all GeV measurements, with the forward-shock emission and for a wind-like medium is shown in Fig 2, with a sequence of spectra shown in Fig 3. The $\chi^2_\nu = 5.7$ for 135 dof of that best-fit makes it statistically unacceptable; the GeV fit has the largest $\chi^2_\nu = 7.1$ for 9 points, closely followed by the optical fit's $\chi^2_\nu = 6.3$ for 39 points, with the largest contribution to the fit's χ^2 arising from the X-ray data, $\Delta\chi^2 = 392$ for 79 points. The model light-curves follow well all flux trends and relative intensities except the brightness of the prompt emission until 50 s, but cannot describe well the early GeV light-curve and cannot capture the fluctuations in the X-ray and optical measurements (after 10 ks, optical data are from different instruments).

2.4 A very tenuous wind

Compared to the parameters inferred for other afterglows by modelling their multiwavelength emission, the wind density of the best-fit shown in Fig 2 is very small, but not unprecedented (Chevalier, Li & Fransson 2004). Its parameter, $A = 0.003$, corresponds to a stellar mass-loss rate – to – terminal wind-velocity ratio (\dot{M}/v) that is 300 smaller than for a typical Wolf-Rayet (WR) star (as the progenitor of long bursts with an associated Type Ic supernovae), for which $\dot{M} = 10^{-5} \dot{M}_{-5} M_\odot/\text{yr}$ and $v = 10^8 v_8$ cm/s. The reason for that low density is the requirement that the synchrotron peak crosses the optical after 3 ks and matches the optical flux detected at that time. For $z = 0.34$ and for the fluid moving directly toward the observer, the forward-shock synchrotron peak energy and peak flux are

$$h\nu_p(10 \text{ ks}) = 0.5 E_{54}^{1/2} \epsilon_{B,-5}^{1/2} \epsilon_{i,-1}^2 \text{ eV} \quad (3)$$

$$F_p(10 \text{ ks}) = 240 E_{54}^{1/2} \epsilon_{B,-5}^{1/2} A \text{ mJy} \quad (4)$$

Imposing that $\nu_p(10 \text{ ks}) = \nu_o = 2$ eV and $F_p(10 \text{ ks}) = F_o(10 \text{ ks}) = 2$ mJy, yields

$$E_{54}^{1/2} \epsilon_{B,-5}^{1/2} \epsilon_{i,-1}^2 = 0.011, \quad E_{54}^{1/2} \epsilon_{B,-5}^{1/2} A = 2.6 \times 10^{-5} \quad (5)$$

Taking the ratio of these two equations leads to $A = 2.3 \times 10^{-3} \epsilon_{i,-1}^2$. The ϵ_i parameter that quantifies the typical electron energy corresponds to a total electron energy that is a fraction $\epsilon_e = (p-1)/(p-2)\epsilon_i$ of the post-shock energy. Equipartition with protons sets an upper limit, $\epsilon_e \leq 1/2$, thus $\epsilon_i \leq 0.12$ for $p = 2.32$, from where $A \lesssim 0.003$.

This wind density is about 20 times lower than the lowest value measured (Nugis & Lamers 2000) for Galactic WR stars and indicates a low mass loss-rate combined with a

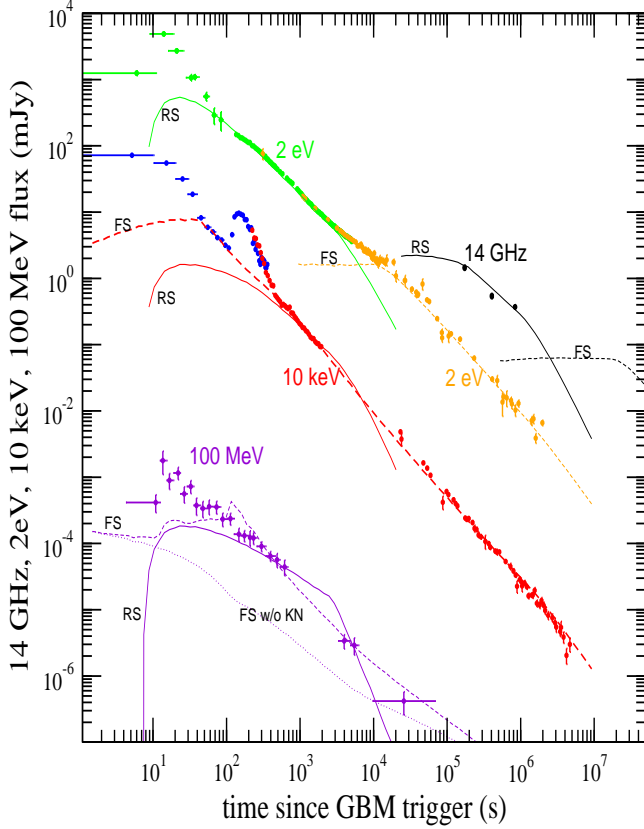


Figure 2. Best-fit with a hybrid reverse(RS)/forward(FS) shock model for the broadband emission of GRB 130427A and for a *wind-like* medium. Solid lines are for the reverse-shock light-curves, dashed lines for the forward-shock; the dotted line shows the 100 MeV forward-shock flux when the Klein-Nishina effect is ignored.

RS parameters: at 10s–3ks: leading ejecta energy $E_0 = 10^{54}$ erg/sr, incoming ejecta energy $E_i^{(1)} = 4.10^{53}$ erg/sr ($E_i^{(1)} < E_0$, hence the dynamics of the forward-shock is not affected by this first energy injection episode), incoming ejecta Lorentz factor $\Gamma_i = 1800$, wind-density parameter $A = 0.004$ (see text for why such a low density is required), $\epsilon_B = 10^{-3}$, $\epsilon_i = 0.011$, $p = 2.0$; at 3ks–1Ms: same E_0 and A as above, $E_i^{(2)} = 4.10^{54}$ erg/sr ($E_i^{(2)} > E_0 + E_i^{(1)}$, thus this second energy injection mitigates the blast-wave deceleration), $\Gamma_i = 3000$, $\epsilon_B = 2.10^{-5}$, $\epsilon_i = 0.016$, $p = 2.3$. The RS optical, X-ray, and GeV emissions (not shown) for the latter injection episode are dimmer than from the FS at same time.

FS parameters: same E_0 , $E_i^{(2)}$ and A as above, $\epsilon_B = 2.10^{-5}$, $\epsilon_i = 0.14$, $p = 2.3$. (Laskar et al 2013 have found almost the same low wind density, with similar ϵ_e and p , but an ϵ_B close to equipartition and an ejecta kinetic energy that is 1000 times smaller).

high wind velocity. Provided that can happen at the end of a WR’s life, it has a strong consequence on the medium in which that star resides, as following. Owing to low wind density and high ejecta kinetic energy, the forward-shock that fits the late time broadband emission of GRB 130427A is highly relativistic, having $\Gamma \simeq 80(t/1\text{ d})^{-1/4}$, hence the shock radius is $R_a = 2\Gamma^2 ct = 8(t/1\text{ d})^{1/2}$ pc. Requiring that R_a at the latest observation epoch (50 day) is less than the size of the bubble blown by a WR star during

its 10^6 yr lifetime, $R_s = 36(\dot{M}_{-5}v_8^2/n_0)^{1/5}$ pc (cf. Castor, McCray & Weaver 1975), with n the medium density around the star, we find that $n \lesssim 5.10^{-4}v_8^3(t_s/50\text{ d})^{-5/2}\text{ cm}^{-3}$ for a wind with $\dot{M}_{-5}/v_8 = 0.004$, where t_s is the observer-frame epoch when the afterglow shock encounters the wind termination shock. Such a low ambient density suggests that the progenitor of GRB 130427A occurred in a super-bubble (Scalo & Wheeler 2001) blown by many preceding supernovae.

2.5 Novel details of the forward-shock model, both related to the high-energy LAT emission

There are two interesting facts related to the LAT emission produced by the forward-shock synchrotron model shown in Figs 1 – 3. First is that the scattering of the synchrotron emission (at the peak of the spectrum) by the forward-shock electrons (of typical energy) occurs near the Klein-Nishina (KN) regime. When the electron cooling is dominated by inverse-Compton scatterings (i.e. Compton parameter $Y > 1$), the cooling frequency satisfies $\nu_c \propto Y^{-2}$. Inclusion of the KN effect reduces the Compton Y parameter, thus, taking into account the KN effect, increases ν_c and the synchrotron flux at $\nu > \nu_c$: $F_\nu \propto \nu_c^{1/2} \propto Y^{-1}$. In other words, the synchrotron emission from fast-cooling electrons increases when a competing radiative process (inverse-Compton) is reduced (by inclusion of the KN effect).

For the forward-shock best-fit to GRB 130427A, the LAT range is above ν_c and $Y > 1$; inclusion of the KN effect reduces Y by about 10 and increases the 100 MeV flux by an order of magnitude (see Fig 2). Furthermore, as the electrons at the peak of their distribution with energy enter and exit the KN regime, the synchrotron light-curve at 100 MeV displays more structure than when the KN effect is ignored.

The second is that radiative cooling during one gyration time limits the energy that electrons acquire through first-order Fermi acceleration to a corresponding synchrotron characteristic energy $h\nu_* \simeq 60(z+1)^{-1}\Gamma/(Y+1)$ MeV, independent of the magnetic field B . For the best-fit parameters given in Fig 2, the forward-shock has $\Gamma(1\text{ ks}) = 240$ and $Y(1\text{ ks})18$, so the maximal synchrotron energy is $h\nu_*(1\text{ ks}) \simeq 600$ MeV (see synchrotron spectrum cut-off in Fig 3). At earlier times, that cut-off is higher, but the inverse-Compton emission from the forward-shock takes over above 2 GeV (as shown by the $t = 75$ s spectrum) and can account for the higher-energy LAT emission until about 10 ks, after which the inverse-Compton flux is too low.

Interestingly, a hardening of the LAT spectrum above several GeV was identified by Tam et al (2013), from $\beta_g^{(low)} = 1.2 \pm 0.1$ at 0.1–5 GeV to $\beta_g^{(high)} = 0.4 \pm 0.2$ at 5–100 GeV. Tam et al (2013) have proposed that the harder high-energy component is inverse-Compton, although we find that the observed spectrum above 5 GeV is softer than the model expectation $\beta_g^{(high)} = -1/3$, corresponding to the GeV range being below the peak of the upscattered spectrum.

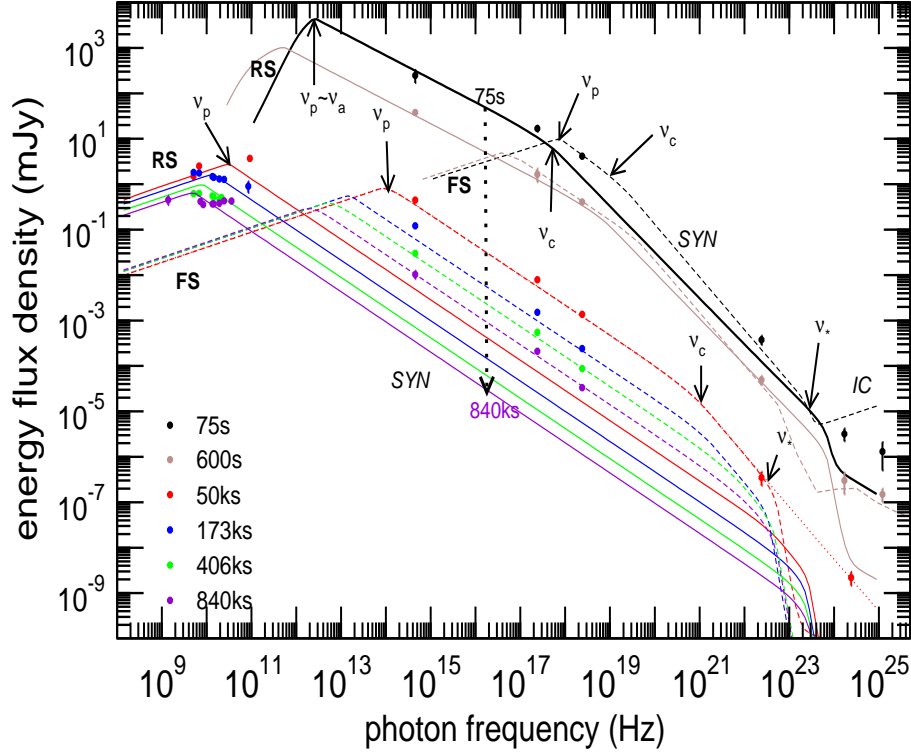


Figure 3. Sequence of spectra for the reverse-forward shock model of Fig 2, at the epochs indicated in the legend. Data at same epoch and the corresponding model spectrum have the same colour, solid lines are for the reverse-shock, dashed for the forward-shock. The spectral breaks indicated are: ν_a (self-absorption frequency), ν_p (peak frequency, for electrons of typical post-shock energy, parametrized by ϵ_i), ν_c (cooling frequency, corresponding to electrons whose radiative cooling timescale equals the shock's age), and ν_* (cut-off frequency, corresponding to electrons that lose their energy during one gyration). The dotted line shows the fit to the 50 ks γ -ray spectrum obtained with the synchrotron FS emission if the electron acceleration timescale were much shorter than the gyration time. The forward-shock inverse-Compton emission emerges above the synchrotron cut-off, yielding a harder spectrum above a few GeV and accounting for the higher-energy LAT emission until several ks.

2.6 Reverse-shock emission for the radio and early optical afterglow

The estimation of the expected radio emission given in equation (2) led to the conclusion that the forward-shock cannot account for the optical afterglow emission prior to ~ 10 ks. Also, the flat radio light-curve arising from the forward-shock interacting with a wind cannot account for the radio emission at 1–10 day, which is slowly decaying. Both these emissions are attributed to the reverse-shock (see also Laskar et al 2013), as discussed below. We note that, after 10 ks, the existence of a reverse-shock is required by the energy injection into the forward-shock required by the measured decay index of the X-ray flux.

The radio data are contemporaneous with the higher energy (optical, X-ray, and γ -ray) afterglow emission accommodated by the forward-shock, thus, for the calculation of the reverse-shock emission, the dynamical parameters E_0 , $E_i^{(2)}$, e , and A are fixed at the values determined from the forward-shock best-fit. The free parameters of the reverse-shock are the Lorentz factor Γ_i of the incoming ejecta (which sets the post-shock energy density) and the three microphysical parameters (ϵ_B , ϵ_i , and p) that determine the synchrotron spectrum. The best-fit obtained with the reverse-shock emission to the 1–10 day radio data is shown in Figs 2 and 3. Unfortunately, it has a large $\chi^2_\nu = 25$ for 25 dof,

because it underestimates the radio flux above 50 GHz. As shown in Fig 3, those radio data cannot be explained by the forward-shock either, if its microphysical parameters are constant. Requiring the same microphysical parameters for both the reverse and forward shocks yields a much worse radio data fit, with $\chi^2_\nu = 47$.

The best-fit to the early optical emission with a reverse-shock includes also the earlier X-ray data and all GeV data, to ensure that the reverse-shock emission does not exceed what was observed. Again, the dynamical parameters E_0 and A are fixed to the values obtained for the forward-shock, but the energy $E_i^{(1)}$ carried by the incoming ejecta arriving at the blast-wave prior to 10 ks is only weakly constrained by the forward-shock fit to the optical and X-ray data after 10 ks, which sets an upper limit $E_i^{(1)} < E_0$. With free micro-parameters, the best-fit with the reverse-shock to the early afterglow has $\chi^2_\nu = 5.4$ for 136 dof, as it fails to account for the GeV prompt emission prior to 100 s, although it explains well the early optical data and the X-ray data at 0.5–3 ks. We note that the reverse-shock magnetic parameter ϵ_B prior to 10 ks (from fitting the early optical afterglow) is 100 times larger than after 10 ks (from modelling for the radio emission). If the reverse-shock microphysical parameters were held constant across 10 ks, then the fit to the radio emission would have a χ^2_ν twice larger, thus a decrease in ϵ_B

at 10 ks is required. That may mean that the ejecta arriving at the blast-wave later are less magnetized.

2.7 Other models with a more complicated afterglow medium structure

As discussed in §2.3, to reconcile the radio and optical fluxes of afterglow 130427A requires that the peak of the forward-shock synchrotron crosses the optical after 3 ks. In turn, that requires (§2.4) a very weak stellar wind, about 300 less tenuous ($\dot{M}_{-5}/v_8 = 0.004$) than for the average Galactic WR star. Then, the forward-shock radius is $R_a(3\text{ ks}) = 1.5\text{ pc}$, while the wind bubble radius should be $R_s = 12(v_8^3/n_0)^{1/5}\text{ pc}$. Thus, if the circumstellar medium is sufficiently dense, it is possible that $R_a(3\text{ ks}) = R_s$. Alternatively, if the stellar wind had the average density, the wind termination shock could be encountered by the forward-shock at 3 ks, provided that the burst is embedded in a hot, highly pressurized environment (Chevalier et al 2004). At frequencies below the cooling break, the afterglow light-curve should display a flattening when the forward-shock crosses the wind termination shock, transiting from the r^{-2} free wind to the quasi-homogeneous shocked wind.

To be self-consistent, the interpretation of the 3 ks optical light-curve flattening as the blast-wave encountering the wind termination shock should attribute the entire afterglow emission to the same shock. Then, the peak of the synchrotron spectrum must be below optical at all times when a decaying optical flux is measured, a model which overproduces radio emission, if the optical afterglow originates in the forward-shock (as shown in §2.3). The subsequent steepening of the optical light-curve at 20 ks cannot originate in the ambient medium stratification because, outside the termination shock, the shocked wind and circumstellar medium are still homogeneous. Instead, that light-curve steepening should be attributed to the cooling frequency falling below the optical, which yields a steepening of the power-law flux decay by $\delta\alpha = 1/4$ (consistent with that measured for the optical light-curve of 130427A at 20 ks), and a softening of the optical spectrum by $\delta\beta = 1/2$ (consistent with the reddening reported by Perley et al 2013, after 10 ks).

The fortuitous temporal coincidence of the cooling frequency falling below optical just after the blast-wave arrives at the free-wind termination shock is not required if the discontinuity in the ambient medium structure that yields the 3 ks optical light-curve flattening is caused by an internal interaction within an unsteady stellar wind or by the interaction between the winds of two stars. In the former scenario, considered analytically by Chevalier & Imamura (1983) and in the context of GRB afterglows by Ramirez-Ruiz et al (2005), a stronger wind produced by the WR star prior to its core-collapse interacts with a slower wind ejected previously. In the latter scenario, proposed by Mimica & Giannios (2011) to be the source for more diverse afterglow light-curves, the GRB progenitor is in a dense stellar cluster, where the mean distance between stars is below 1 pc, and the WR wind interacts with the weaker wind of a nearby O star or a later type. In either scenario, after the interaction with the shocked wind(s), which yields a light-curve flattening, the blast-wave goes into an r^{-2} wind, which is the earlier WR wind or the wind of the nearby star, producing

a light-curve steepening, with the flux decay index α returning to the value it had during the interaction with the free WR wind. Only the dense cluster scenario provides a natural explanation for the very weak wind inferred here from modelling the afterglow 130427A: the wind of a B star located within 1 pc of the GRB progenitor. However, this scenario cannot explain why that weak wind extends over tens of pcs (as required by the duration of the afterglow, §2.4) despite the more powerful winds of nearby, earlier type stars.

Thus, the 3 ks flattening and 20 ks steepening seen in the optical light-curve of 130427A could originate from a forward-shock interacting with the more complex ambient medium resulting from an internal wind interaction provided that microphysical parameters evolve such that this model does not exceed the 1–10 day radio measurements. Alternatively, radio emission is not overproduced if the entire afterglow emission arises from the reverse-shock, and the optical light-curve flattening and steepening could result from the changing dynamics of the reverse-shock when the shocked-wind shell is crossed. Such light-curve features could also be due to variations in the density and Lorentz factor of the incoming ejecta, without any need for a non-uniform ambient medium.

However, a model where the entire afterglow emission arises from the same shock (reverse or forward) does not provide a natural explanation for the colour evolution displayed by 130427A, which becomes bluer after 3 ks (Vestrand et al 2013), when the optical light-curve flattens, and redder after 10 ks (Perley et al 2013), when the optical light-curve steepens. In contrast, the hybrid reverse-forward shock model explains naturally both the 3 ks spectral hardening, as due to the harder (below the synchrotron peak energy) forward-shock emission emerging from under the softer reverse-shock emission, and the following spectral softening, caused by the peak energy of the forward-shock synchrotron spectrum falling below optical.

3 CONCLUSIONS

The closure relations expected between the forward-shock synchrotron flux decay index and spectral slope suggest a homogeneous ambient medium for GRB afterglow 130427A. Although long GRBs arise from massive stars that drive powerful winds, a homogeneous medium is possible if the afterglow emission is produced in the shocked wind. However, this afterglow's (10 ks) optical flux to (1–10 day) radio flux ratio and its slowly decaying radio light-curves disfavour that type of mbient medium. Instead, for an unevolving constant magnetic field parameter, the synchrotron spectrum peak flux is constant and the radio emission should have been brighter and slowly rising. With some fine-tuning of the evolutions of those micro-parameters, it may be possible to reduce the forward-shock model radio flux below measurements, while still accounting for the observed optical and X-ray light-curves.

A wind-like medium ($n \propto r^{-2}$) is the more natural expectation for a massive star as the GRB progenitor. The forward-shock emission still cannot account for the radio data because the expected radio light-curve is flat, however, a wind-like medium yields a decreasing synchrotron spec-

trum peak flux, making it easier to keep the forward-shock radio emission below radio measurements. To explain the optical and X-ray flux decay after 10 ks with the forward-shock synchrotron emission, a moderate energy injection into the forward-shock is required, increasing the shock energy by a factor 4 from 10 ks to 1 Ms. The agent of that energy injection should be some ejecta that arrive at the forward-shock at that time, which provides a natural explanation for the afterglow radio emission: the reverse-shock that crosses the incoming ejecta.

The reverse-shock must have been operating at even earlier times because the high early-optical to late-radio flux ratio precludes a forward-shock origin of the optical afterglow emission prior to 10 ks. Such a reverse-to-forward shock switch for the origin of the optical emission, occurring at few ks, is supported by the optical afterglow becoming bluer^{*} at that time (Vestrand et al 2013), when the forward-shock emission, with a spectrum $F_\nu \propto \nu^{1/3}$ in the optical, begins to dominate the softer reverse-shock emission, with a spectrum $F_\nu \propto \nu^{-1/2}$. As the peak of the forward-shock synchrotron spectrum falls below optical at about 10 ks, the optical afterglow should become redder after 10 ks, as was observed by Perley et al (2013).

However, for the reverse-shock to explain the 100 s – few ks optical afterglow and the 1–10 day radio afterglow emission, the properties of the reverse-shock (microphysical parameters, kinetic energy and Lorentz factor of the incoming ejecta) must change around 10 ks. Furthermore, Vestrand et al (2013) have shown that the reverse-shock can also account for the optical flash (up to 100 s) and the GeV light-curve peak, but for microphysical different than after that peak.

For this hybrid reverse-forward shock model, we find that the X-ray flux of GRB afterglow 130427A is accounted mostly by the forward-shock emission, from the tail of the first GRB pulse (50–100 s) up to 5 Ms, excluding the second GRB pulse at 100–500 s. The reverse-shock may have had a significant contribution to the early X-ray emission, at 500 s – 2 ks. Both shocks give comparable GeV emissions. As shown in Fig 2, the radio emission from the forward-shock is expected to overshadow that from the reverse-shock at 30 day (or somewhat later, if energy injection continues after 1 Ms), yielding a flat flux $\lesssim 0.1$ mJy until ~ 200 day, when the peak of the synchrotron spectrum falls below 10 GHz. If that flat radio flux is not seen, then the magnetic field parameter ϵ_B of the forward-shock must be decreasing, so that the peak flux of the forward-shock synchrotron spectrum falls off faster than the $F_p \propto t^{-1/2}$ expected for $\epsilon_B = \text{const}$.

The relative dimness of the radio afterglow suggests that the peak of the synchrotron spectrum has crossed the optical range at 10 ks. An immediate consequence is that the wind-like ambient medium is a factor 20 less dense than the most tenuous wind measured for Galactic WR stars. We cannot provide a good argument for why GRB 130427A's progenitor had such a low mass-loss rate –to– wind-speed ratio ($\dot{M}/v = 4 \times 10^{-11} (\text{M}_\odot/\text{yr})/(\text{km/s})$), but note that,

owing to the weak wind, the afterglow remains highly relativistic and travels ~ 100 pc until the last observation epoch (50 day). For such a large afterglow radius to remain inside the free WR wind (i.e. within the wind termination shock), the GRB progenitor must have been embedded in a very tenuous medium, suggesting a super-bubble blown by preceding supernovae and stellar winds.

Owing to tenuous ambient medium, the afterglow transverse size, $2R_\perp = 2\Gamma ct \simeq 0.1(t/1\text{d})^{3/4}$ pc, is unusually large, and implies a source apparent diameter of $\theta = 0.63(t/100\text{d})^{3/4}$ mas, which may be resolved with radio interferometry.

If the GeV emission of GRB afterglow 130427A arises from the forward-shock, then the up-scattering of the synchrotron emission occurred at the onset of the KN regime, where the reduction of the electron scattering cross-section lowers the Compton parameter, increases the synchrotron cooling-break frequency, and increases the synchrotron flux above that break (i.e. in the LAT range). Furthermore, LAT must have measured the forward-shock inverse-Compton emission at photon energies above a few GeV.

ACKNOWLEDGMENTS

This work was supported by an award from the Laboratory Directed Research and Development programme at the Los Alamos National Laboratory and made use of data supplied by the UK Swift Science Data Centre at the University of Leicester.

REFERENCES

- Blandford R., McKee C., 1976, *Phys. Fluids*, vol 19, 1130
- Castor J., McCray R., Weaver R., 1975, *ApJ* 200, L110
- Chevalier R., Imamura J., 1983, *ApJ*, 270, 554
- Chevalier R., Li Z., 2000, *ApJ*, 536, 195
- Chevalier A., Li Z., Fransson C., 2004, *ApJ* 606, 369
- Evans P. et al, 2009, *MNRAS*, 2009, 397, 1177
- Granot J., Piran T., Sari R., 1999, *ApJ*, 527, 236
- Kennea J. et al, 2013, *GCN Circ.*, 14485
- Kobayashi S., 2000, *ApJ*, 545, 807
- Kobayashi S., Sari R., 2000, *ApJ*, 542, 198
- Laskar T. et al, 2013, *ApJ*, 776, 119
- Mimica P., Giannios D., 2011, *MNRAS*, 418, 583
- Mészáros P., Rees M., 1997, *ApJ*, 476, 232
- Nugis T., Lamers H., 2000, *A&A* 360, 227
- Panaitescu A., Mészáros P., 1998, *ApJ*, 492, 683
- Panaitescu A., Kumar P., 2000, *ApJ*, 543, 66
- Panaitescu A., Mészáros P., 2000, *ApJ*, 544, L17
- Panaitescu A., 2005, *MNRAS*, 363, 1409
- Perley D. et al, 2008, *ApJ*, 672, 449
- Perley D. et al, 2013, *ApJ*, preprint (arXiv:1307.4401)
- Ramirez-Ruiz E. et al, 2005, *ApJ*, 631, 435
- Rees M., Mészáros P., 1998, *ApJ*, 496, L1
- Sari R., Piran T., Narayan R., 1998, *ApJ*, 497, L17
- Scalo J., Wheeler J., 2001, *ApJ*, 562, 664
- Tam P. et al, 2013, *ApJ*, 771, L13
- Vestrand T. et al, 2013, *Science*, submitted
- Waxman E., Kulkarni S., Frail D., 1998, *ApJ*, 497, 288
- Wijers R., Galama T., 1999, *ApJ*, 523, 177
- Woźniak P. et al, 2009, *ApJ*, 691, 495
- Zhu S. et al, 2013, *GCN* 14508

^{*} This feature, accompanied by a flattening of the optical flux decay, was previously observed in two other GRB afterglows: 061126 (Perley et al 2008) and 080319B (Woźniak et al 2009)